



U-Pb direct dating on calcite paleosol nodules: first absolute age constraints on the Miocene continental succession of the Paris Basin

Vincent Monchal¹, Rémi Rateau¹, Kerstin Drost¹, Cyril Gagnaison², Bastien Menecart³, Renaud Toullec², David Chew¹

5 ¹Geology, School of Natural Sciences, Trinity College Dublin, Dublin, D02 PN40, Ireland

²Département Géosciences, Unité Bassins-Réservoirs-Ressources (B2R-U2R 7511), Institut Polytechnique UniLaSalle Beauvais, UniLaSalle-Université de Picardie, Beauvais, 30313, France

³Naturhistorisches Museum Basel, Basel, 4001, Switzerland

10 *Correspondence to:* Vincent Monchal (monchalv@tcd.ie)

Abstract

Continental sedimentary successions are typically less complete and more poorly preserved than the marine record, leading to limited correlations between basins. Traditionally, intra-basin correlation employs radiometric dating of volcanic markers or relative dating based on the fossil record. However, volcanic markers may not always be present, and biostratigraphy relies on index fossils which are often sparse to absent in continental successions. Recent progress in carbonate U-Pb dating can improve correlations between continental successions by providing absolute age constraints on carbonate deposition and/or on syn- to post-depositional processes such as pedogenesis.

In this study, we analysed pedogenic calcite nodules within a continental Miocene succession in the southwestern Paris Basin (the important paleontological site at Mauvières quarry, France). Following multimethod petrographic characterisation of the samples, LA-ICP-MS U-Pb dating was employed to obtain formation ages on the pedogenic calcite nodules. The Tera-Wasserburg intercept ages from five nodules from the same horizon (19.3±1.3/1.4 Ma, 18.0±3.2/3.2 Ma, 19.11±0.84/0.94 Ma, 19.0±2.3/2.3 Ma and 19.4±2.7/2.7 Ma) are in excellent agreement with previous biostratigraphic constraints on the sequence. Petrographic evidence points to a single crystallisation event, and we conclude that the formation of the calcite nodules occurred at 19.34 ± 0.58/0.73 Ma (central age from a radial plot of the five Tera-Wasserburg intercept ages). This calcite formation age is regarded to represent a minimum depositional age of the strata hosting the root nodules. It provides the first direct age for the continental Miocene succession (and Neogene mammal zone MN3) of the Paris Basin and allows correlation with other continental basins independent of their fossil assemblages or when the fossil content is missing.



1 Introduction

30 Biostratigraphy assigns relative ages to rock strata by using the fossil assemblages contained within them, with the goal of showing that a particular horizon in a given section represents the same period of time as the same horizon in a different succession. It relies heavily on the presence of index fossils - fossils with a limited time range, wide geographic distribution, and rapid evolutionary trends. The common absence of biostratigraphically-diagnostic index fossils in continental successions is problematic, and absolute dating approaches often need to be applied to continental successions. Such approaches include
35 geochronology of volcanic horizons such as lava flows or ash beds (e.g., Rubidge et al., 2013; Poujol et al., 2023), astronomic calibration (e.g., Kerr 1992, Montano et al., 2021), and magnetostratigraphic correlation (e.g., Kalin and Kempf 2009). While volcanic horizons can provide accurate and precise absolute ages, they are not ubiquitous in the sedimentary record. Carbonates are very common in terrestrial successions where they can be classified as pedogenic or non-pedogenic, depending on whether they have formed by soil-forming processes (Zamanian et al., 2016). Pedogenic carbonates comprise calcretes and dolocretes
40 - paleosols that have been indurated by a pervasive calcitic cement; pisoliths - globular nodules made of concentric calcitic spheres; and more generic calcitic nodules - indurated concretions with a globular or cylindrical shape, often associated with calcitic cementation around plant roots (rhizocretions; Zamanian et al., 2016).

U-Pb dating of calcium carbonate started in the late 1980s using isotope dilution (ID) – thermal ionisation mass spectrometry (TIMS) methods (Smith and Farquhar, 1989; Roberts et al., 2020 and references therein). Most terrestrial U-Pb carbonate
45 dating studies have focused on non-pedogenic carbonates (e.g. speleothems, tufas and lacustrine carbonates; see review in Rasbury and Cole, 2009). The first U-Pb dating studies applied to terrestrial pedogenic carbonates took place in the mid-1990s on Paleozoic uranium-rich dolocretes, developed subaerially on top of marine limestones (Hoff et al., 1995; Winter and Johnson, 1995). Over the following years, a series of ID-TIMS U-Pb dating studies yielded meaningful subaerial exposure ages from 1) Late Paleozoic paleosol-derived sparry calcite developed on top of marine carbonate cyclothem in the
50 southwestern USA (Rasbury et al., 1997, 1998, 2000; Rasbury and Cole, 2009); 2) Late Paleozoic dolocretes from Kansas, USA (Luczaj and Goldstein, 2000); 3) Late Paleozoic subaerially soil-modified palustrine limestones in Ohio, USA (Becker et al., 2001); and 4) Triassic calcretes developed on top of fluvial siliciclastics deposits in Connecticut, USA (Wang et al., 1998) (Table 1).

Since the mid-2010s, advances in laser ablation inductively coupled plasma mass spectrometry (LA-ICP-MS) have allowed
55 U-Pb dating of carbonates with the benefits of much greater spatial resolution, mineralogical context (being in-situ), and sample throughput (e.g., Li et al., 2014; Roberts and Walker, 2016; Nuriel et al., 2017). While individual LA-ICP-MS spot ablation U-Pb data are typically significantly less precise than ID-TIMS U-Pb analyses, the high spatial resolution of the approach means it can commonly encounter both high and low U/Pb portions of the sample, resulting in age regressions with superior precision compared to ID-TIMS U-Pb dating studies which employ bulk sampling (e.g., Li et al., 2014). The technique has
60 been employed to date pedogenesis including 1) Eocene pedogenic calcite nodules from Montana, USA (Methner et al., 2016) and 2) Ediacaran dolomite from subaerially weathered volcanics in Ukraine (Liivamägi et al., 2021) (Table 1).



Age	$\pm 2\sigma$	MSWD	Max. U	Technique	Material dated			Soil protolith	Reference
					Country	Rock	Mineral		
39.5	1.4	0.89	3.25	LA-SF-ICP-MS (spots)	USA	Pedogenic nodule	Cal.	clastics & volcanics - continental	Methner <i>et al.</i> , 2016
40.1	0.8	1.15	3.44	LA-SF-ICP-MS (spots)	USA	Pedogenic nodule	Cal.	clastics & volcanics - continental	Methner <i>et al.</i> , 2016
80.9	11	30	0.6	ID-TIMS	USA	Rhizolith	Cal., blocky	clastics - fluvatile	Wang <i>et al.</i> , 1998
211.9	2.1	2.67	2.7	ID-TIMS	USA	Calcrete	Cal., micritic	clastics - fluvatile	Wang <i>et al.</i> , 1998
212.4	3.4	3.4	2.5	ID-TIMS	USA	Calcrete	Cal., micritic	clastics - fluvatile	Wang <i>et al.</i> , 1998
254	29	504	29	ID-TIMS	USA	Dolocrete	Dol.	carbonates - marine	Luczaj and Goldstein, 2000
275	6	?	?	ID-TIMS	USA	Paleosol	Cal.	carbonates - lacustrine?	Becker <i>et al.</i> , 2001
282	28	417	32.5	ID-TIMS	USA	Dolocrete	Dol.	carbonates - marine	Hoff <i>et al.</i> , 1995
294	6	?	?	ID-TIMS	USA	Paleosol	Cal.	carbonates - lacustrine?	Becker <i>et al.</i> , 2001
294.9	8.6	2.2	~27	LA-Q-ICP-MS (map)	USA	Calcrete	Cal., sparry	carbonates - marine	Rasbury <i>et al.</i> , 2023
298.1	1.4	0.9	8.6	ID-TIMS	USA	Calcrete	Cal., sparry	carbonates - marine	Rasbury <i>et al.</i> , 1997, 1998, 2000, 2009
306	2.6	0.6	-	ID-TIMS	USA	Calcrete	Cal., sparry	carbonates - marine	Rasbury <i>et al.</i> , 1998
512	10	314	1.24	ID-TIMS	USA	Dolocrete	Dol.	carbonates - marine	Winter and Johnson, 1995
548	19	1.3	0.57	LA-SF-ICP-MS (spots)	Ukraine	Weathered volcanics	Dol., blocky	volcanics - basalts, tuffs	Liivamägi <i>et al.</i> , 2018

Abbreviations: Cal. = Calcite, Dol. = Dolomite, ID-TIMS = Isotope Dilution Thermal Ionization Mass Spectrometer, LA-(SF-/Q-)/ICP-MS = Laser Ablation (Sector Field/Quadrupole) Inductively Coupled Mass Spectrometry

Table 1: Summary of published U-Pb ages of terrestrial pedogenic carbonates (modified and updated after Rasbury and Cole, 2009).

LA-ICP-MS U-Pb dating requires chemically homogenous and large enough zones (typically, between 50 and 200 μm wide circles or squares) to obtain sufficient U and radiogenic Pb signals to produce meaningful age results (Roberts and Holdsworth, 2022). Additionally, high U and low common Pb concentrations are required to produce precise U-Pb dates, but carbonates typically incorporate low U concentrations (unless the precipitation takes place in reducing environments, e.g Fournier *et al.*, 2004; Drake *et al.*, 2018) and significant common Pb (Roberts *et al.*, 2020). Carbonates in general and pedogenic carbonates in particular, are also often heterogenous at the hundreds of micron scale or below (Zamanian *et al.*, 2016; Roberts and Holdsworth, 2022), partially explaining the paucity of reliable dating results from pedogenic carbonates. More widespread absolute dating of pedogenic carbonates could provide valuable chronostratigraphic constraints in continental successions, particularly those where volcanic horizons or index fossils are absent.

A recent and innovative LA-ICP-MS U-Pb carbonate dating protocol, based on the selection and pooling of pixels from 2D elemental and isotopic ratio maps (Drost *et al.*, 2018; Roberts *et al.*, 2020; Chew *et al.*, 2021) is now commonly employed as a U-Pb dating strategy (e.g. Monchal *et al.*, 2023; Rasbury *et al.*, 2023; Subarkah *et al.*, 2024). This in-situ technique allows for the selection of chemically homogenous zones within a chemically heterogenous ablated 2D map area, reducing the risk of incorporating U-Pb data from non-carbonate inclusions or different generations of carbonates (Drost *et al.*, 2018). In addition, this method optimises the spread of data points in Tera-Wasserburg (TW) space increasing the precision of the results (Drost *et al.*, 2018). Therefore, this mapping-based technique is well suited to U-Pb dating and elemental characterisation of paleosol calcite, and would help alleviate some of the issues caused by microheterogeneity in pedogenic carbonates. A late Paleozoic paleosol calcite, already dated by ID-TIMS (298.1 \pm 1.4 Ma; Rasbury *et al.*, 1998) has been successfully dated using this approach (294.9 \pm 8.6 Ma; Rasbury *et al.*, 2023).

Continental sedimentary successions are often barren or poor in index fossils, which makes dating and intra-basin correlation difficult. Mammal remains have been used to create terrestrial biostratigraphic scales, such as the Neogene mammal (MN) scale in Western Europe (Mein, 1975; Agustí *et al.*, 2001). The European MN scale is similar to the North American Land Mammal “Ages” (NALMAs) and South American Land Mammal “Ages” (SALMAs) scales (see the review of Hilgen *et al.*,



2012). However, mammal fossils are not ubiquitous in the sedimentary record, thus the MN and other mammal scales cannot always be employed. When compared to marine biostratigraphic records (which have index fossils such as planktonic foraminifera, ammonites, graptolites etc.), they also exhibit diachronicity and a poorer temporal resolution. The poor temporal resolution, particularly in the early stages of the MN scale (see Discussion) is well illustrated by the MN3 biozone, which has a duration of between 2.8 and 5.4 Myr, depending on the absolute age chosen for the top and bottom boundaries (Mein, 1999; Steininger, 1999; Aguilar et al. 2003; Raffi et al., 2020). For comparison, the Paleogene calcareous nannofossil scale biozones all have a duration lower than 2 Myr, with most lower than 1 Myr (Agnini et al., 2014). The LA-ICP-MS calcite U-Pb geochronology approach adopted herein could have the potential to constrain the age of continental sedimentary horizons where pedogenic nodules are present, improve inter-basins correlations and better constrain the temporal resolution of the MN scale, potentially highlighting regional diachronism. In this study, we apply the LA-ICP-MS U-Pb mapping technique along with spot analysis to obtain absolute ages from pedogenic calcite nodules from a terrestrial Miocene succession in the Paris Basin, France, whose age is hitherto poorly constrained in terms of direct dating.

2 Geological setting

100 2.1 Regional geology

The Mauvières paleontological site is located in the SW of the Paris Basin (France), a Mesozoic-Cenozoic intracontinental sag basin (Guillocheau et al., 2000). The site is on the northeast margin of the Neogene outcrops, which comprise continental and marine sedimentary rocks unconformably deposited on Paleogene continental sedimentary rocks (Figure 1a). Regionally, the Cenozoic sedimentary sequence reflects a dominantly continental paleoenvironment with occasional marine transgressions during the Miocene (Figure 1b, Gagnaison, 2020).

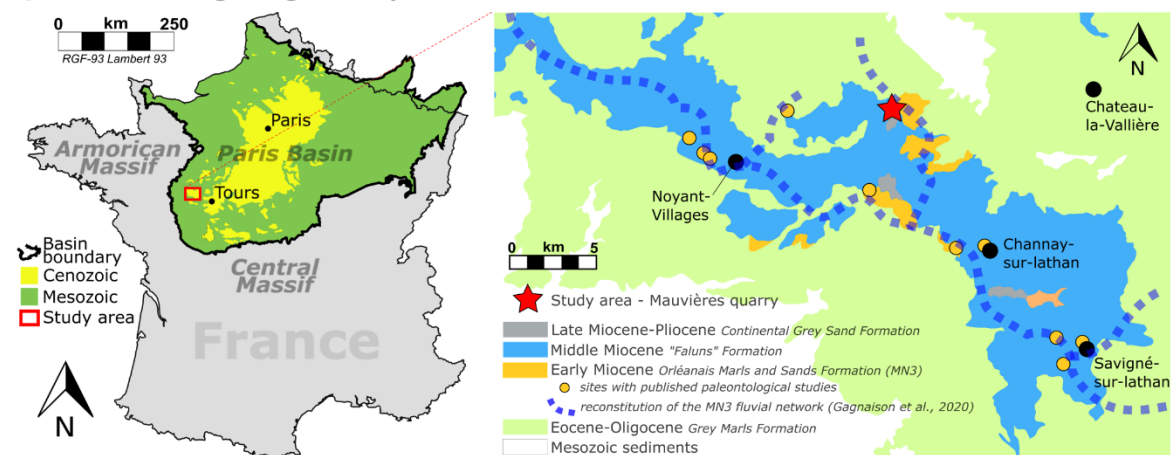
2.2 Paleoenvironment and origin of the calcite nodules

The pedogenic nodules were sampled from the Early Miocene (early to middle Burdigalian) Orléanais Marls and Sands Formation (Figure 1b), a few meters-thick succession of coarse and fine-grained clastic sediments (Figure 2). This formation rests unconformably over a Paleogene lacustrine silty marl (the Eocene-Oligocene Grey Marls Formation) and is overlain by Middle Miocene marine shelly carbonate sands, known locally as “*faluns*” (Gagnaison et al., 2023) (Figure 1b and Figure 2). The Early Miocene continental sequence at Mauvières consists of a series of eight clastic beds (numbered s1 to s8; Gagnaison et al., 2023; Figure 2a). The pedogenic nodules were found in the basal bed s1, which overlies Paleocene-Eocene silty marls (Figure 2). The s1 bed is comprised of a very coarse light grey-orangey quartzitic sand with minor feldspar, in-situ terrestrial vertebrate fossils, poorly preserved *Unio* shells (a freshwater mussel), and in-situ carbonate nodules and cylinders. The sand also contains reworked material, including Cretaceous calcareous and siliceous pebbles, altered glauconite grains and Cretaceous and Oligocene / Early Miocene vertebrate fossils. The sand is loosely cemented with a clayey and calcareous matrix

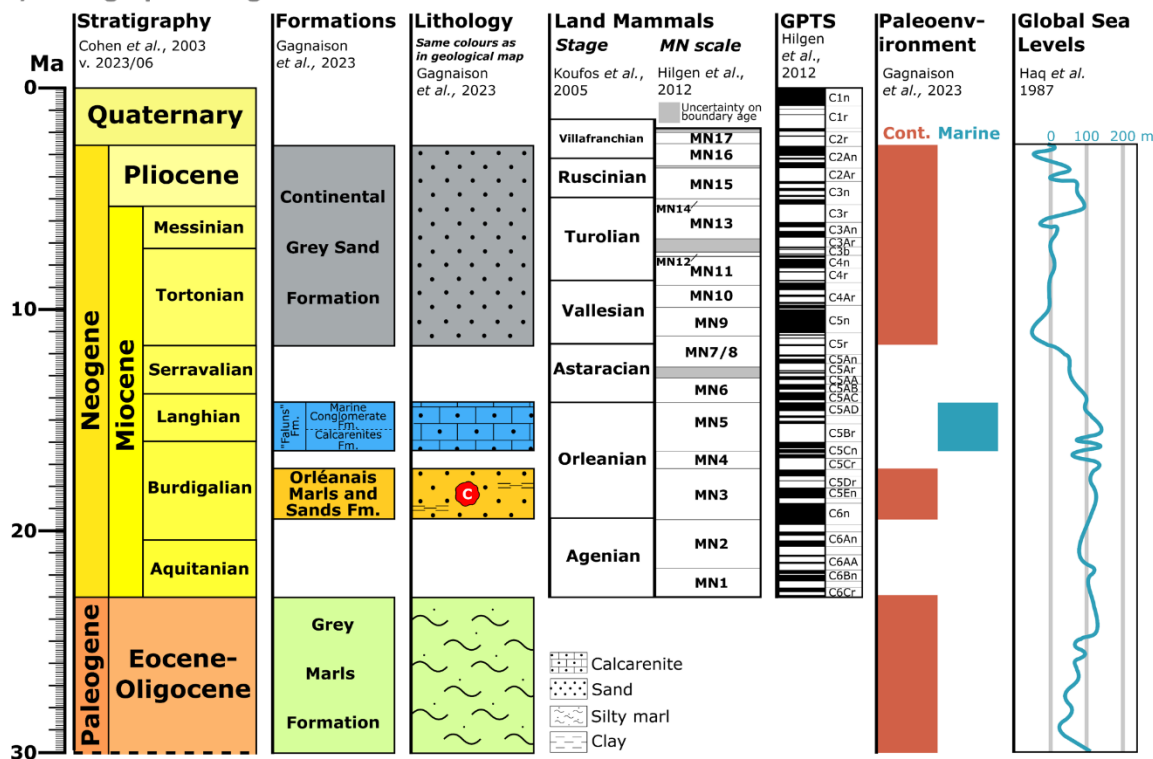


(Gagnaison et al., 2023). Some rare *Unio* shells have been found with both valves still connected, indicating both a low-energy environment and that they are in-situ (i.e. not reworked from older beds).

a) Location and geological map



b) Stratigraphic range chart



120 Figure 1: Geological context of the Mauvières section. a) Location of the Mauvières quarry and regional geology based on the BRGM 1/50,000 unified vector geological map of France (InfoTerre), modified after Gagnaison et al. (2020). b) Stratigraphy of the Mauvières section. The nodules (red symbol) come from the Orléanais Marls and Sands Formation attributed to the MN3 biozone (Gagnaison et al., 2023).



The occurrence of 1) hollow calcite cylinders and nodules interpreted as rhizcretions, 2) root tracks in the matrix, 3) iron oxides which give the orange colour to the sand, and 4) microvacuoles interpreted as subaerial microbial activity, suggests the presence of a paleosol (Gagnaison et al., 2023). The nodule-bearing s1 bed is interpreted as a water-transported, low-energy fluvial sequence with prograding sand bars, with phases of lacustrine floodings and development of paleosols. The sequence was subsequently subaerially exposed and followed by the development of a vegetated soil (Gagnaison et al., 2023). The pedogenic nodules are consequently interpreted as in-situ and not reworked from older horizons. Rasbury et al. (1997) have shown that the calcite typically forms rapidly following paleosol development, and therefore absolute dating of the nodules should provide robust age constraints on the s1 bed.

2.3 Biostratigraphic age of the continental sands and nodule-bearing s1 bed

MN biozones were defined as a tool for inter-basin faunal comparisons (Mein, 1999). Limits of the zones are defined by 1) steps in mammalian evolutionary lineages (local evolution), 2) First Appearance Datum and/Last Appearance Datum of species, 3) dispersal of taxa, and 4) faunal assemblages (Mein, 1999; Steininger, 1999). As discussed by Mein (1999), even when relatively inaccurate, the MN-zones are still a useful tool for regional correlation. For example, where local mammalian biozones are developed (e.g. the Mongolian Mammalian biostratigraphy proposed by Daxner-Höck et al., 2017), the MN system can still be employed since Europe and Asia often share taxa (Wang et al. 2013). However, we should keep in mind that correlation using the MN timescale is affected by ecological limits, latitudinal disparities, general diachronism in the dispersion of taxa, the presence of immigrant taxa (Mein 1999; Steininger, 1999) and local differences in taxa (even between neighbouring basins; Engesser and Mödden 1997).

Regionally, both the continental and marine Miocene sediments are known for their rich fauna of vertebrate fossils, including mammal taxa (Ginsburg, 2001). At Mauvières, vertebrate remains have been found within four horizons within the Orléanais Marls and Sands Formation (Figure 2a). The majority of fossils (>95%) are fresh and thus interpreted as syn-sedimentary and not reworked from older beds. In total, 53 taxa have been identified, most of them present in the s1 bed, the richest of the four fossiliferous horizons. The taxa are typical of the middle of the MN3 biozone (Gagnaison et al., 2023) (Figure 1b and Figure 2a).

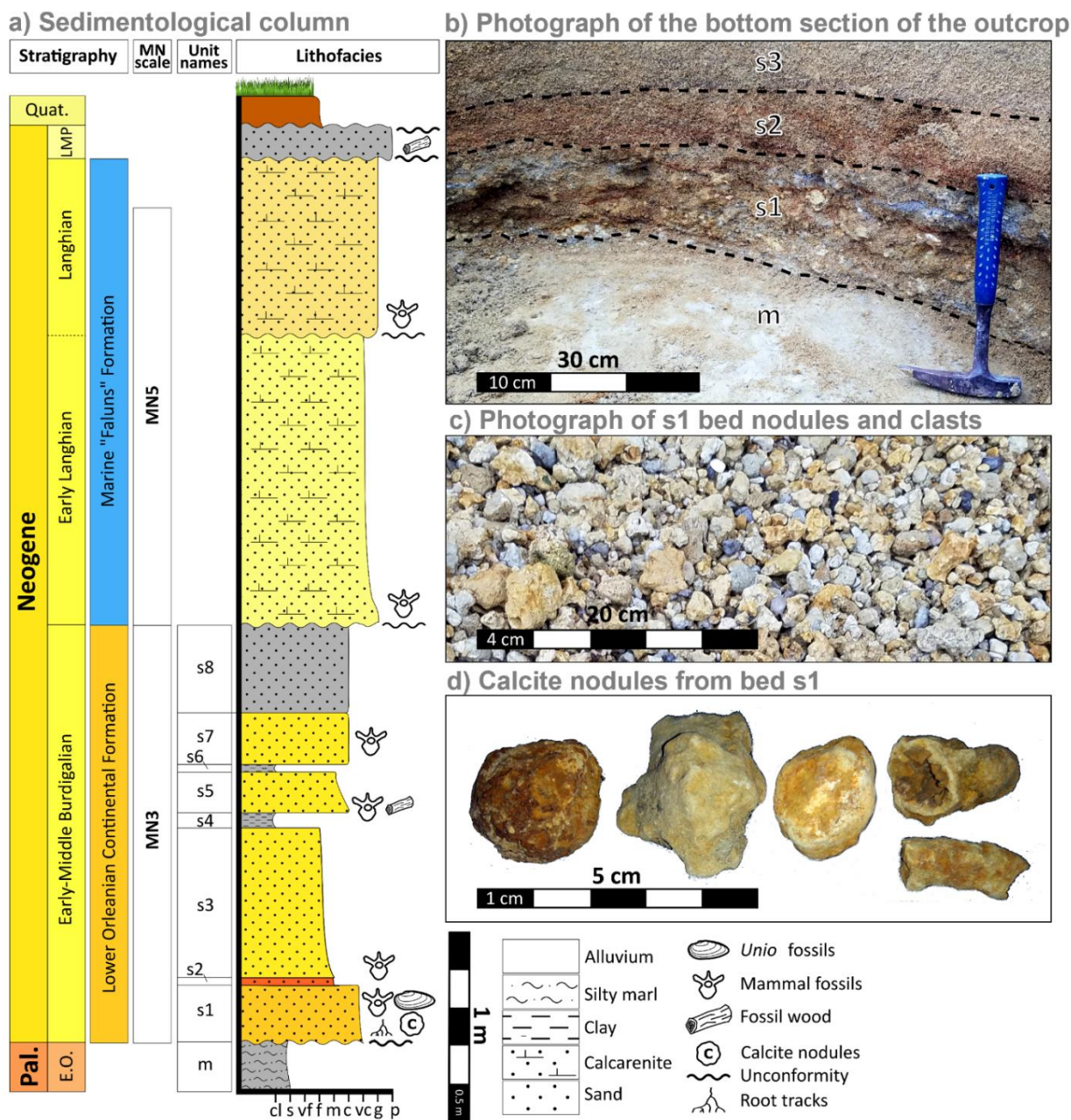


Figure 2: Geology of the Mauvières section. a) Sedimentological log and bed nomenclature (modified after Gagnaison et al., 2023). The calcite nodules are found in the Early-Middle Burdigalian basal sand s1. b) Photograph of the basal section of the outcrop, showing the basal Paleocene-Eocene silty marls unconformably overlain by an orange, very coarse fluvial sand with mammal remains, freshwater mussel shells, root tracks and pedogenic calcite nodules. c) Granule and pebble fraction after sieving of the s1 sand. The fraction is dominated by pale-coloured calcite nodules. d) Photographs of representative calcite nodules from the s1 bed showing both spherical and cylindrical irregularly-shaped nodules of varying colour.



3 Materials and methods

155 3.1 Samples

Between 2020 and 2022, a series of geological sampling campaigns were undertaken at the Mauvières site. The sample material was sieved, washed, and dried. From the coarse separate (>2 mm), numerous nodules were collected and identified as vadose carbonate nodules (Gagnaison et al., 2023). The nodules are spherical to oblong, with a yellow-orange colour and a coarse aspect. Five of these nodules were selected for SEM elemental analysis and U-Pb dating (P00, P01, P02, P04 and P14), three
160 nodules for powder X-ray diffraction analysis (XRD), and one nodule was prepared as a thin section for detailed microscopic analysis (MIOC4). For XRD analysis, each selected nodules were crushed in an agate mortar to create a fine powder. The five
165 other nodules selected for U-Pb dating were sawn in half to reveal an internal surface. One half of each nodule was mounted in a 25 mm mould, mounted in epoxy resin, cured and polished, with the final polishing step employing 1 µm diamond suspension polishing fluid. The epoxy resin mounts were cleaned in an ultrasonic bath of deionized water for three minutes
and imaged by optical microscopy. LA-ICP-MS U-Pb dating was undertaken on sample P00 to see if high quality age data can
be obtained from the sample suite. Following LA-ICP-MS analysis of sample P00, it was repolished to remove the ablation
rasters, cleaned in an ultrasonic bath of deionized water and carbon coated for SEM analysis. The other four samples were first
carbon coated for SEM analysis, and later polished then cleaned to remove the carbon before subsequent LA-ICP-MS analysis.

3.2 Optical microscopy

170 The resin pucks were imaged under reflected light using a Nikon Eclipse LV100 at the iCRAG Lab@TCD, Trinity College
Dublin. Images were acquired at 5x magnification using a Nikon DS-Ri2 camera. Each tiled image is comprised of multiple
frames stitched together by the Nikon NIS-Elements software. Each frame was taken with a square field of view of c. 2.8 mm
in width and with an overlap of 10%. Transmitted and plane-polarised light images were also acquired for thin section MIOC4.

3.3 XRD

175 The powders were analysed using a Siemens/Bruker D5000 power X-ray diffractometer (Cu K α radiation, 0.01° step⁻¹ from
5 to 60° 2 θ at 1° min⁻¹, 4.5 hours per sample). Mineral identification was undertaken with DIFFRAC.EVA (Bruker) using the
Powder Data File (PDF-4, The International Centre for Diffraction Data) (Gates-Rector and Blanton, 2019).

3.4 SEM

The SEM analyses were carried out at the iCRAG Lab@TCD (Trinity College Dublin, Ireland) on a Tescan TIGER MIRA3
180 FEG-SEM equipped with a backscatter electron detector (BSE), two Oxford Instruments Ultim Max 170 mm² SSD EDX
detectors and an X4 pulse processor. Scanning electron (SE) and BSE imaging and energy-dispersive X-ray spectroscopy
(EDS) analyses were acquired using an accelerating voltage of 20 keV and a working distance of 15 mm above the carbon-



coated pucks. The images and maps were processed using the AZtec version 6.1 X-ray microanalysis software suite (Oxford Instruments).

185 3.5 LA-Q-ICP-MS

Laser ablation Q(quadrupole)-ICP-MS U-Pb dating was performed at iCRAG Lab@TCD, Trinity College Dublin, employing an Iridia 193 nm ArF excimer LA system (Teledyne Photon Machines, Bozeman, MT, USA) coupled to an Agilent 7900 Q-ICP-MS via 1.016mm ID PEEK tubing and a medium pulse interface. One sample (P00) was dated using a mapping approach and follows the U-Pb imaging technique described in Drost et al. (2018), while the remaining samples (P00-repeat, P01, P02, 190 P04, P14) were analysed by static spot analysis. For the latter, signal smoothing was achieved by inserting a mixing chamber (Glass Expansion) between medium pulse interface and torch. Details on the specific analytical protocol and operating conditions are given in the supplementary material (Supplementary Table 1-6 and Supplementary Document 1). This includes the selection criteria, regions of interest, map dimensions and time-equivalents for all selected pixels and pixel groups ('pseudo-analyses') for the sample analysed with the mapping approach, and the laser pit locations of the samples analysed by spot 195 ablation. Supplementary Tables are available on Zenodo repository system (Monchal et al., 2024) while Supplementary Document and Figure are available with the online version of this manuscript.

Samples were first screened for suitability using line scans. Samples and sample area yielding high initial Pb concentrations and low μ throughout were omitted from further analysis. Similarly, samples areas with $U \leq 10$ ppb were ignored as the young sample age would result in very low concentrations of radiogenic Pb. Final locations for U-Pb analysis were selected according 200 to the results of the test line scans in combination with mineralogical and textural observations from optical microscopy and from chemical information obtained by SEM-EDS mapping. In each dated nodule, we targeted calcite zones with minimal incorporation of other phases. For the mapping experiment, this resulted in multiple groups of raster lines spread out across the nodule surface. Final ROIs for data extraction were chosen to represent zones that could be interpreted as cogenetic and thus a single age population constraining cementation. However, samples P01, P02, P04, and P14 did not feature large enough 205 coherent calcite areas with Pb/U ratios favourable for efficient and reproducible use of the mapping protocol. Spot analysis was subsequently performed on those samples, using the chemical information from the SEM and LA-ICP-MS maps to help site the spot analyses. Additionally, the U-Pb mapping data from sample P00 was also augmented by a static spot ablation experiment.

The mapping session employed a laser spot size of 80 μ m square, a repetition rate of 50Hz and a fluence of 2.5J/cm² while 210 moving the sample along successive linear rasters with 30 μ m/s under the static laser beam. Samples were bracketed by NIST614 glass as the primary standard, WC-1 calcite for matrix-matching the ²⁰⁶Pb/²³⁸U ratio (Roberts et al., 2017) and Duff Brown Tank limestone as quality control material (Hill et al., 2017). The total analysis time for sample P00 was c. 34 minutes. Spot analysis employed 85 μ m diameter spots, a repetition rate of 12 Hz, 480 shots (40s) and a fluence of 2.2J/cm². Again, NIST614 was used as the primary standard, but Duff Brown Tank limestone was used for matrix-matching of the ²⁰⁶Pb/²³⁸U



215 ratio as it is closer in U concentration and age to the samples than WC-1. Gas settings (optimised daily), analyte menus and
integration times for all analytical sessions are reported in Supplementary Doc 1 along with the data processing protocols used.
Uncertainties on dates in the text and figures are quoted at the 2σ or 95% confidence level, respectively. The geochronological
results are presented with two uncertainties; the first is an estimate of the session uncertainties, while the second is propagated
with full systematic uncertainties (e.g., the uncertainty on the reference age of WC-1 (maps) or DBT (spots) respectively, the
220 decay constant uncertainties, and the 2% long-term reproducibility of secondary age reference materials in the laboratory; see
Supplementary Document 1).

4 Results

4.1 Petrographic observations

The samples are composed of transparent, mostly rounded quartz grains with some more angular crystals, set in a pale orange-
225 yellow cement with vein-like cavities, partially filled with carbonate crystals (Figure 3). The majority of the samples exhibit a
main cavity that sometimes branches out *via* micro-cracks, typical of alpha type paleosol (Wright, 1990). We can distinguish
two stages of formation. The first stage involves the formation of sedimentary concretions around roots. The concretions are
rich in quartz and cemented by clear calcite crystals as observed under the optical transmitted light microscope (Figure 3).
After decomposition of the roots, the carbonate crystals precipitated predominantly into free space producing a brown layer
230 on the edge of the cavity and filling the micro-cracks. The host-rock is composed of touching or floating terrigenous clastic
elements such as quartz in a clotted carbonated matrix with authigenic goethite. The host-rock is also cross-cut by rhizolith
root tubules, traces of which are still visible (Figure 3A). These relics of paleo-roots are expressed by the stack of several
layers of dark microbial micrite linings (Figure 3A) and some holocrystalline microsparite. The presence of holocrystals is
dependent on the degree of microbial activity and the root structure (i.e. main axis *vs* lateral roots). These early pedogenic
235 carbonate crystals (Figure 3B-C) are classically found in many paleosols (e.g. Wright, 1987; Esteban and Klappa, 1983; Bain
and Foos, 1993; Alonso-Zarza, 2003).

Sample MIOC4 is a representative nodule from the s1 bed that exhibits evidence of primarily calcified root traces (Figure 3;
see also Gagnaison et al., 2023). No evidence of later crystallisation nor recrystallisation was detected, with the calcite spar
homogeneous and unzoned (Figure 3B-C). Moreover, micro-cracks and alveolar structures are commonly found without calcite
240 crystallisation (Figure 3A), especially where the primary root was located. When calcite crystals are present, they are typically
associated with lateral roots.

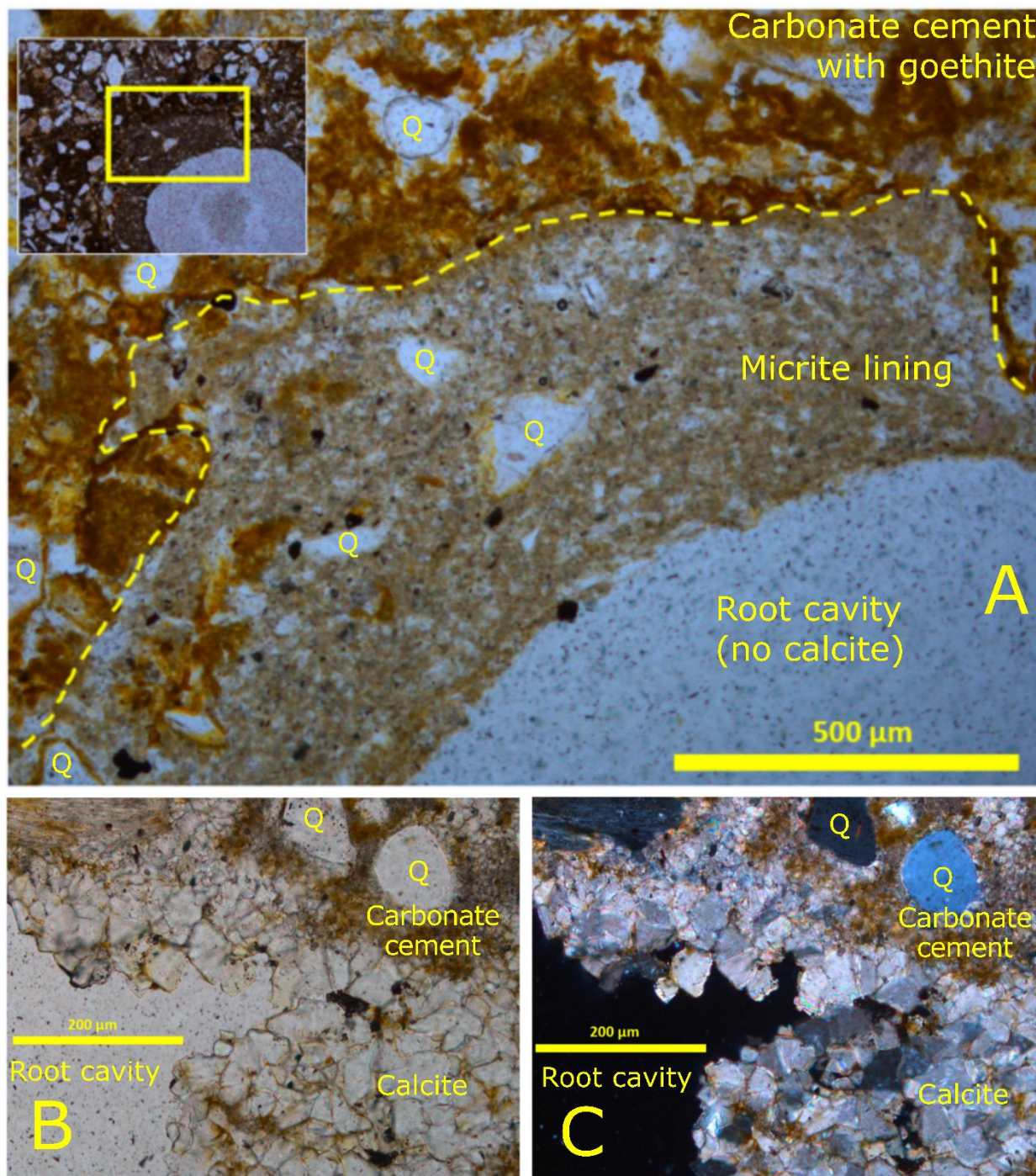


Figure 3: Optical microscope photography of sample MIOC4. A) Primary root structure with a dark microbial micrite lining – dashed yellow line highlights the boundary of the external part of the microbial micrite lining. An alveolar structure can be seen on the zoomed out insert at the top of the microphotograph (PPL). B) Microsparitic carbonate cement; a lateral root perforation is on the lower left side of the microphotograph (PPL) and C) (XPL). Q = Quartz.

245



4.2 Powder XRD phase identification

The PXRD patterns of the three analysed nodules consistently show two dominant families of peaks identified as calcite (e.g., ICDD PDF no. 00-047-1743) and quartz (e.g., ICDD PDF no. 00-046-1045). Minor feldspar (e.g., ICDD PDF no. 00-09-0466[Albite] and 00-19-0932[Microcline]) (Figure 4) and several unidentified minor peaks corresponding to one or more accessory phase(s) in the nodules are also present. The confirmation that the carbonate phase is calcite allows accurate matrix-matching with the WC-1 calcite age reference material in the LA-ICP-MS U-Pb dating procedure (Roberts et al., 2017).

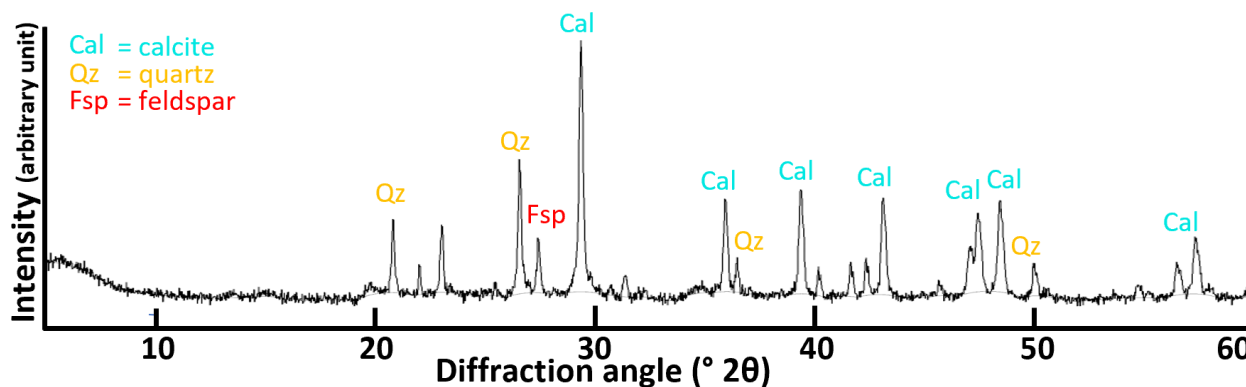
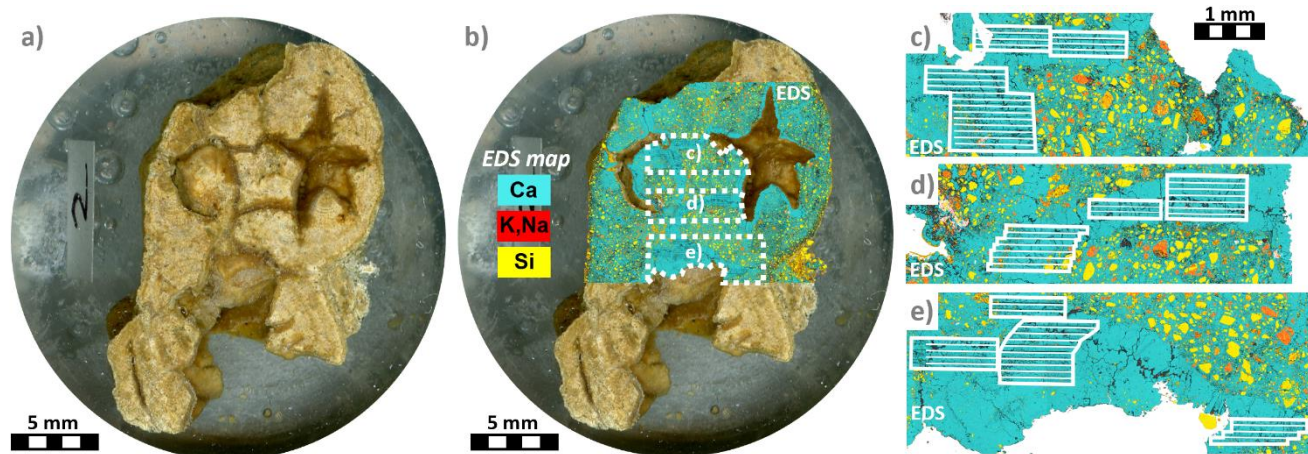


Figure 4: Representative PXRD patterns from a calcite nodule showing the dominance of calcite and quartz.

4.3 SEM-EDS elemental mapping

The SEM-EDS maps of the five dated nodules reveal that the nodules are composed of poorly sorted angular Si-rich minerals cemented by a Ca-rich phase (Figure 5). The two phases are interpreted respectively as quartz and calcite based on optical microscopy and the PXRD results. The cemented sand also contains grains rich in Si and K, Na interpreted as feldspar and in agreement with the results of PXRD. Large cavities, often branching or rounded are present in all the nodules. These cavities are lined by a pure Ca-rich phase interpreted as calcite that precipitated into the free cavity space. In some locations, quartz-free calcite crystals have filled the cavities entirely. These zones of pure calcite were subsequently targeted for LA-ICP-MS U-Pb dating.



265 **Figure 5: Photographic montage of nodule P00 in a polished resin puck. a) optical microscopy image b) the same image overlain by a partial EDS map of the nodule showing Ca (a proxy for calcite, blue), Si (a proxy for quartz, yellow), and K,Na (a proxy for feldspar, red). The location of the EDS maps in c), d), and e) are represented by the dashed white polygons. c), d) and e) EDS maps showing the LA-ICP-MS ablation zones and line scans for the P00 nodule. Pure calcite veins were targeted, avoiding the zones of calcite-cemented quartz-rich sand. See Supplementary Materials for pictures and EDS map of the other samples (Supplementary Figure 1).**

4.4 LA-ICP-MS U-Pb dating

270 Calcite crystals that have precipitated freely inside the cavities were targeted for geochronology analysis (Figure 6) as they are believed to have precipitated rapidly after the formation of the paleosol (see section 2.2 and Rasbury et al., 1997). The mapped areas in P00 targeted zones of pure calcite based on the SEM-EDS mapping. A Ca filter (e.g. retaining pixels with Ca > 350 000 ppm) was applied on the P00 map to exclude any inclusions, cracks, epoxy resin or the host sedimentary rock and this filter removed c. 7% of the pixels from the maps. The average U content is c. 10 ppm (ranging from 9 to 13 ppm), while the average Th content is c. 0.7 ppm (ranging from <0.1 to 2.5 ppm; see Supplementary Table 1) resulting in Th/U ratios of <0.01

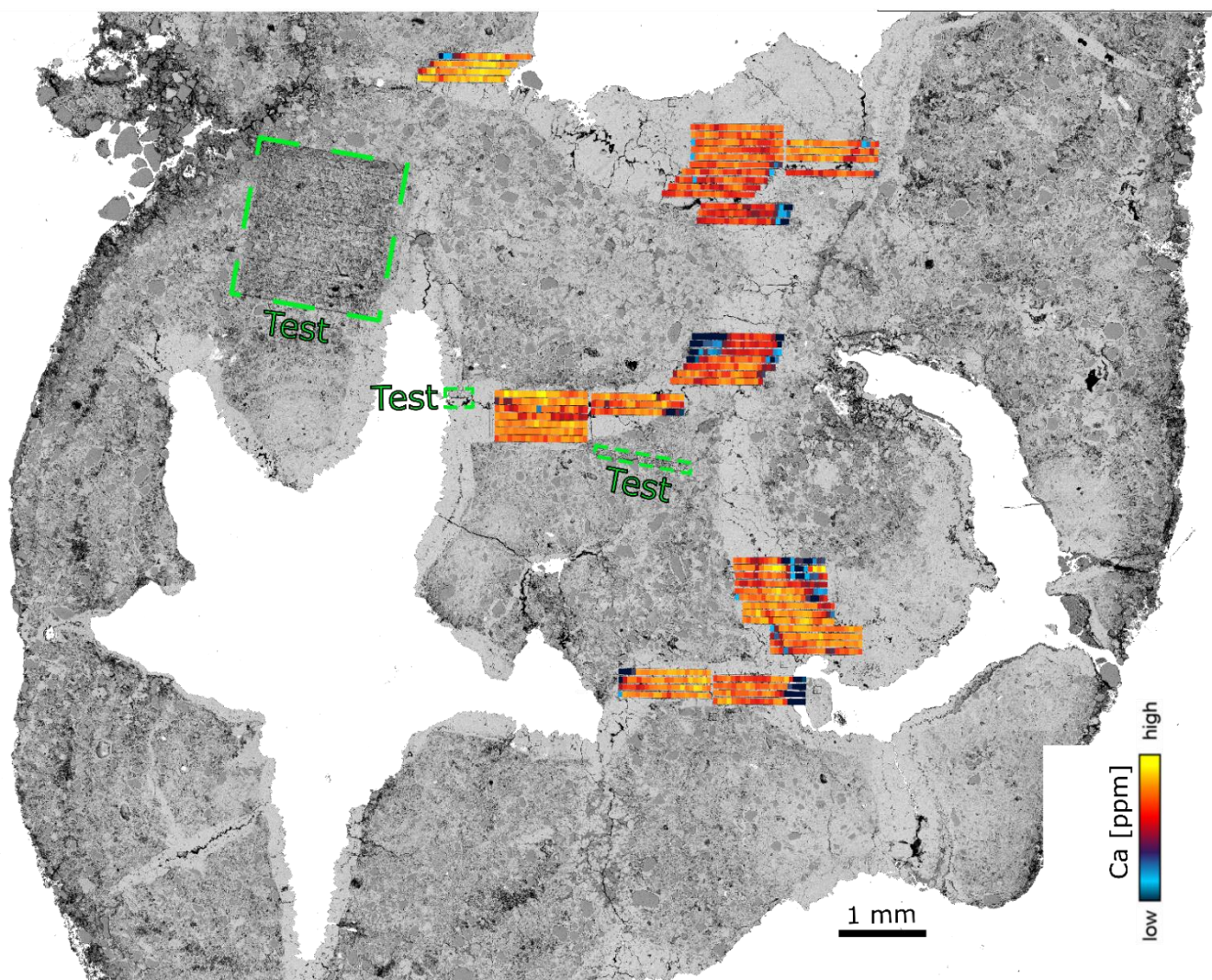
275 to <0.2. Significant initial Pb concentrations (~0.44 to 33ppm) and the long half-life of Th in combination with the young age of the sample render the radiogenic ingrowth of radiogenic ^{208}Pb negligible ($^{208}\text{Pb}_{\text{common}}/^{208}\text{Pb}_{\text{radiogenic}} \sim 2800$ to 12000). Therefore we used the empirical cumulative distribution function of the $^{238}\text{U}/^{208}\text{Pb}$ channel for pooling of the filtered pixel data into pseudo-analyses. The $^{238}\text{U}/^{208}\text{Pb}$ channel is a good estimate of the parent U vs initial Pb (μ) as the total ^{208}Pb concentration strongly reflects the initial $\text{Pb}_{\text{common}}$ component.

280 The spot U-Pb data was corrected post-analysis for any shot that went through the calcite. This correction employ the visual inspection of peaks for a significant change in Ca, Pb, Th or U composition that indicate a change in the phase ablated. The U-Pb spot analyses on samples P01, P02, P04 and P14 yielded dates of $18.0 \pm 3.2/3.2$ Ma, $19.11 \pm 0.84/0.94$ Ma, $19.0 \pm 2.3/2.3$ Ma, $19.4 \pm 2.7/2.7$ Ma, respectively, while sample P00 yielded dates of $19.3 \pm 1.3/1.4$ Ma (mapping) and $20.4 \pm 1.3/1.4$ Ma (spots) (Figure 7). A radial plot and weighted average age were calculated using these six dates and their respective internal

285 uncertainties (session estimates), while the full systematic uncertainties (section 3.5) were propagated onto the resultant age



(radial plot or weighed average) calculation. The radial plot in Figure 8 shows a single age group at $19.34 \pm 0.58/0.73$ Ma ($p[X^2] = 0.68$) and a weighted average age was calculated at $19.32 \pm 0.58/0.73$ Ma (MSWD=0.62; see Figure 8). The radial plot single group age of $19.34 \pm 0.58/0.73$ Ma is the preferred age adopted in this study as discussed in section 5.2.



290 **Figure 6:** BSE image of P00 overlain by the LA-ICP-MS line rasters used to extract the age. This figure shows that the pristine calcite was targeted by our analysis.

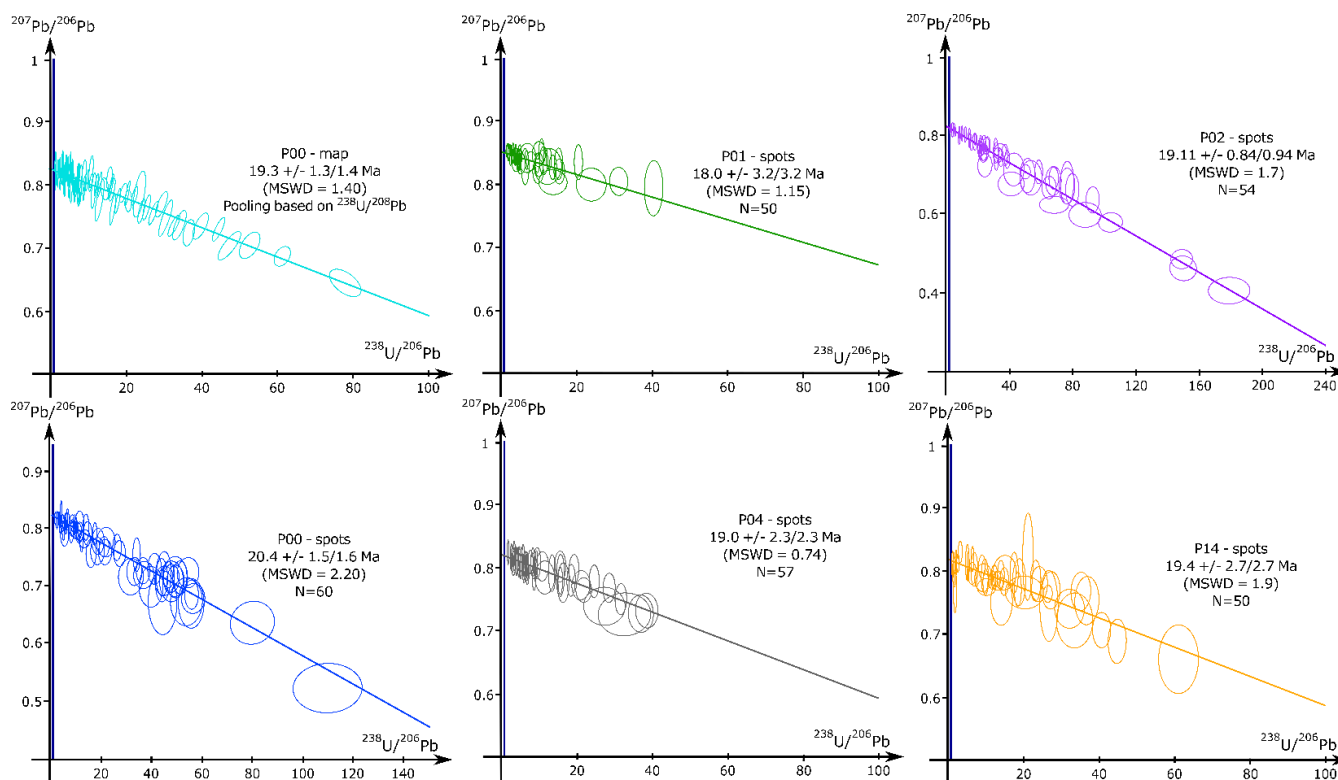
5 Discussion

5.1 Accuracy and precision of the U-Pb ages

The imaging techniques (optical microscopy, SEM-EDS and LA-ICP-MS mapping) have differentiated zones of pristine calcite and the pervasive cementation of the nodules. Optical microscopy evidence favours the hypothesis of preservation of



295 pristine calcite in our samples (see Results section 4.1). In addition, prior to their extraction from the s1 bed, all the pedogenic nodules (along with clasts and fossil material) were coated with an impermeable clay layer, which likely hindered subsequent passage of fluid into the nodules. The clay coating is interpreted as syn-sedimentary (see figures 2b-d and Gagnais et al., 2023). This sealed system is another argument in favour for the preservation of pristine calcite (Perry and Taylor, 2006) in the nodule interiors (See Figures 4 and 5).



300 **Figure 7: Tera-Wasserburg concordia diagrams and lower intercept ages of all samples. For the map analysis of P00, the pooling was based on the ECDF $^{238}\text{U}/^{208}\text{Pb}$. For the spot analysis, the number of spots is indicated by N.**

The LA-ICP-MS mapping technique adopted herein is recognised for its potential (see Rasbury et al., 2023) in dating pedogenic nodules by allowing the selection of only pristine calcite in the extraction and processing of the U-Pb data. However, only one sample had large enough coherent zones of pristine calcite with Pb/U ratios suitable for U-Pb dating and a spot analysis strategy was used to date the remaining four samples. All six analyses yield ages with a precision of 5 to 18%, which is precise for carbonate U-Pb dating of such young samples (Roberts et al., 2020). The accuracy of our data set can be assessed by the fact that the five samples provide the same age and initial $^{207}\text{Pb}/^{206}\text{Pb}$ within uncertainties, along with the radial plot confirming that there is only one age group (Figure 8). The accuracy of the mapping experiment is also demonstrated by the similar ages (within uncertainties) yielded using three different isochron approaches. Sample P00 (using $^{238}\text{U}/^{208}\text{Pb}$ as the pooling channel) yields $19.3 \pm 1.3/1.4$ Ma for the TW intercept age, $19.6 \pm 1.7/1.8$ Ma for the $^{238}\text{U}/^{208}\text{Pb}_{\text{common}}$ isochron (e.g., 310 Getty et al., 2001) and an 86TW age (Parrish et al., 2018) of $19.4 \pm 1.6/1.7$ Ma (section 3.4 and Supplementary Table 1).

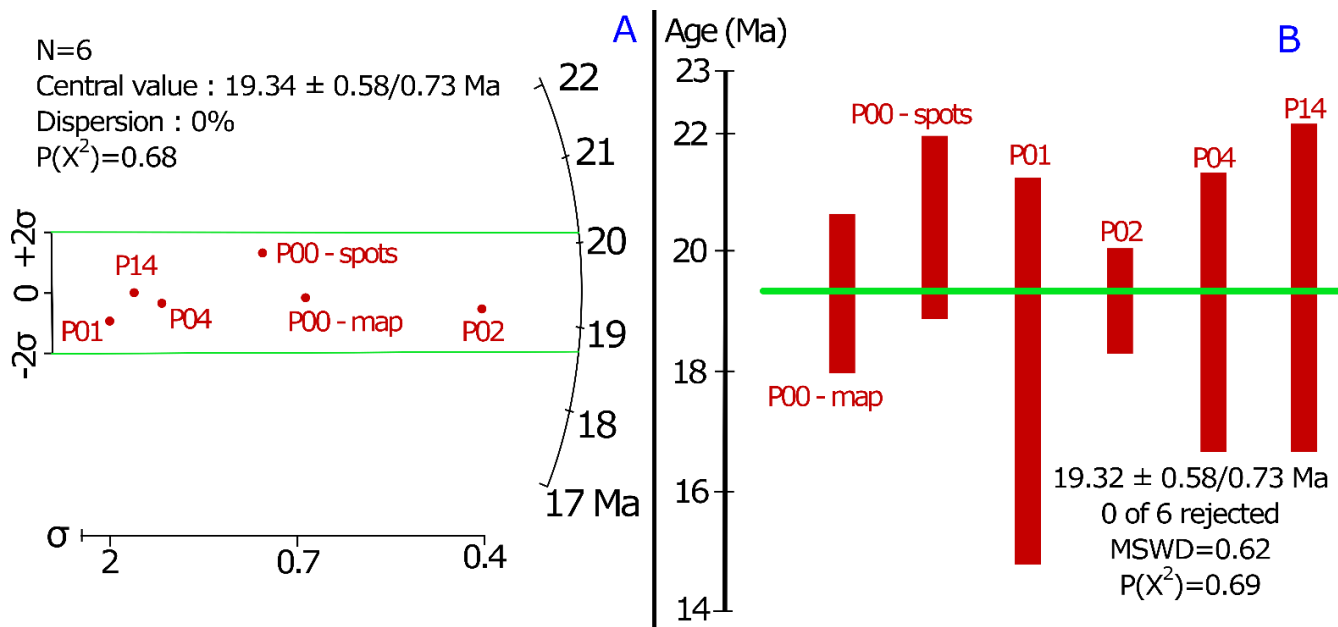


Figure 8: A) Radial plot and B) weighted average of the samples used in this study. Radial plot central value and the weighted average value are indicated with 2σ internal uncertainties (session estimates). The full systematic uncertainties (section 3.5) were propagated onto the resultant age calculations with the same method as for the individual sample ages. See text for the interpretation and discussion of the data.

315

5.2 Age of the nodules and paleosol

Our age data are compatible within uncertainty with the proposed biostratigraphic age of the continental biozone MN3 which is correlated with the Burdigalian marine stratigraphic age (20.44-15.98 Ma; Cohen et al., 2013 [updated 2023/09]) and the Orleanian continental stratigraphic age (19.5-14.2 Ma; Gagnaison et al., 2023). Dating the pedogenic calcite should provide a minimum age for the paleosol formation (Rasbury et al., 1997). The nodules are found within the same sedimentary layer (section 2.2) and we can therefore reasonably assume that the crystallisation of the calcite inside each nodule arose from the same process(es). Even if these process(es) involve multiple phases of growth, we do not see any evidence of incremental growth of more than one generation of calcite from petrography and SEM-EDS mapping.

320

We therefore assume that formation of the analysed nodules (which are identical within age uncertainty of our method) was effectively synchronous. The age of formation of the nodules was statistically determined following the recommendations of Vermeesch (2018) using the radial plot central age of the TW intercept ages from the six experiments. The radial plot shows only one age group, and the central age from the radial plot and the weighted mean of the TW intercept ages are identical within age uncertainty. The weighted mean age calculation assumes the data follows a normal distribution, while the radial plot assumes that the log of the values follows a normal distribution curve (Vermeesch, 2018). Geochronological data are less likely to conform to a normal distribution due to the presence of outliers. The log of the outliers will smooth these deviations and heteroscedastic variation (unequal uncertainties) and make it fit to the normal distribution curve (Galbraith et al. 1999), which is why the radial plot central age is preferred. This age of 19.34±0.58/0.73 Ma for the s1 bed allows precise correlation

330



with other directly dated sequences, independently of the lithofacies or fossil assemblages present. This age is the first absolute
age for the continental Miocene facies of the Paris Basin and to the best of our knowledge the youngest U-Pb age from
335 pedogenic carbonates in the literature (Table 1).

5.3 Biostratigraphic significance

The MN (Mammal Neogene) stratigraphic timescale is based on faunal calibration. The appearance and disappearance of taxa
result in a given combination of species that can be linked to a given time (Mein, 1999). The MN scale incorporates a
stratigraphic component as well as classical stratigraphic correlations and magnetostratigraphy to help refine the age control
340 (Hilgen et al., 2012). MN units were initially defined without boundaries or clearly defined limits (e.g. Mein, 1975), but
nowadays the scale is often presented alongside a chronostratigraphic scale, with an absolute age associated with each biozone
boundary (e.g. Agustí et al., 2001; Van Dam et al., 2001; Aguilar et al., 2003; Gagnaison et al., 2023). The absolute ages of
the boundaries remain debated (see the example of MN3 below) due to diachronicity and incomplete paleontological and
magnetostratigraphical data (Fortelius et al., 2014; Ezquerro et al., 2022). Each zone is characterised by a specific fauna found
345 at a reference locality (for Europe these are mainly in Spain and Switzerland) that can be asynchronous by up to 1-2 Ma in the
Late Miocene (Van der Meulen et al., 2012; Fortelius et al., 2014; Ezquerro et al., 2022). The majority of the MN zones have
uncertainties attached to their age boundaries (Figure 9), while the application of the MN timescale typically involves
comparison to the most proximal and well-constrained reference section to circumvent potential diachronicity. Local
modifications to the MN timescale are thus often adopted for selected biozones (Hilgen et al., 2012; Van der Meulen et al.,
350 2012; Fortelius et al., 2014; Ezquerro et al., 2022).

To improve the precision of this scale, the incorporation of magnetostratigraphy has helped to better define the MN unit
boundaries within basins (e.g. Agusti et al. 2001; Kálin and Kempf 2009). Steininger (1999) used magnetostratigraphic data
to propose that magnetostratigraphic data to propose that magnetostratigraphic data to propose that magnetostratigraphic data
to propose that magnetostratigraphic data to propose that magnetostratigraphic data to propose that magnetostratigraphic data
355 North Alpine foreland (Agusti et al., 2001). The MN3 faunal reference site is Wintershof-West with a sedimentary succession
dated between 17.5 and 18.5 Ma (Hilgen et al., 2012). Refined magnetostratigraphic data to propose that magnetostratigraphic data
dated between 17.5 and 18.5 Ma (Hilgen et al., 2012). Refined magnetostratigraphic data to propose that magnetostratigraphic data
dated between 17.5 and 18.5 Ma (Hilgen et al., 2012). Refined magnetostratigraphic data to propose that magnetostratigraphic data
dated between 17.5 and 18.5 Ma (Hilgen et al., 2012). Refined magnetostratigraphic data to propose that magnetostratigraphic data
360 not challenging the actual consensus around the absolute age of the base or the top of MN3 (Figure 9).



Absolute U-Pb dating of in-situ pedogenic carbonates enables a better understanding of the spatio-temporal distribution and evolution of continental mammalian faunas. This method is not affected by the limits detailed above, thus offering a reliable opportunity to improve the local constrain on MN scale. Our age is compatible with an early Orleanian stage assignment (Figure 1) and the MN3 unit (Hilgen et al. 2012). The age constraints on the Mauvières fossil locality are thus significantly improved by our results, but it should be noted that an age for one locality does not improve the precision of the MN3 boundaries at a European scale. Therefore, more studies employing similar method are needed for further improvement of the MN scale, especially zones with large uncertainties such as MN3.

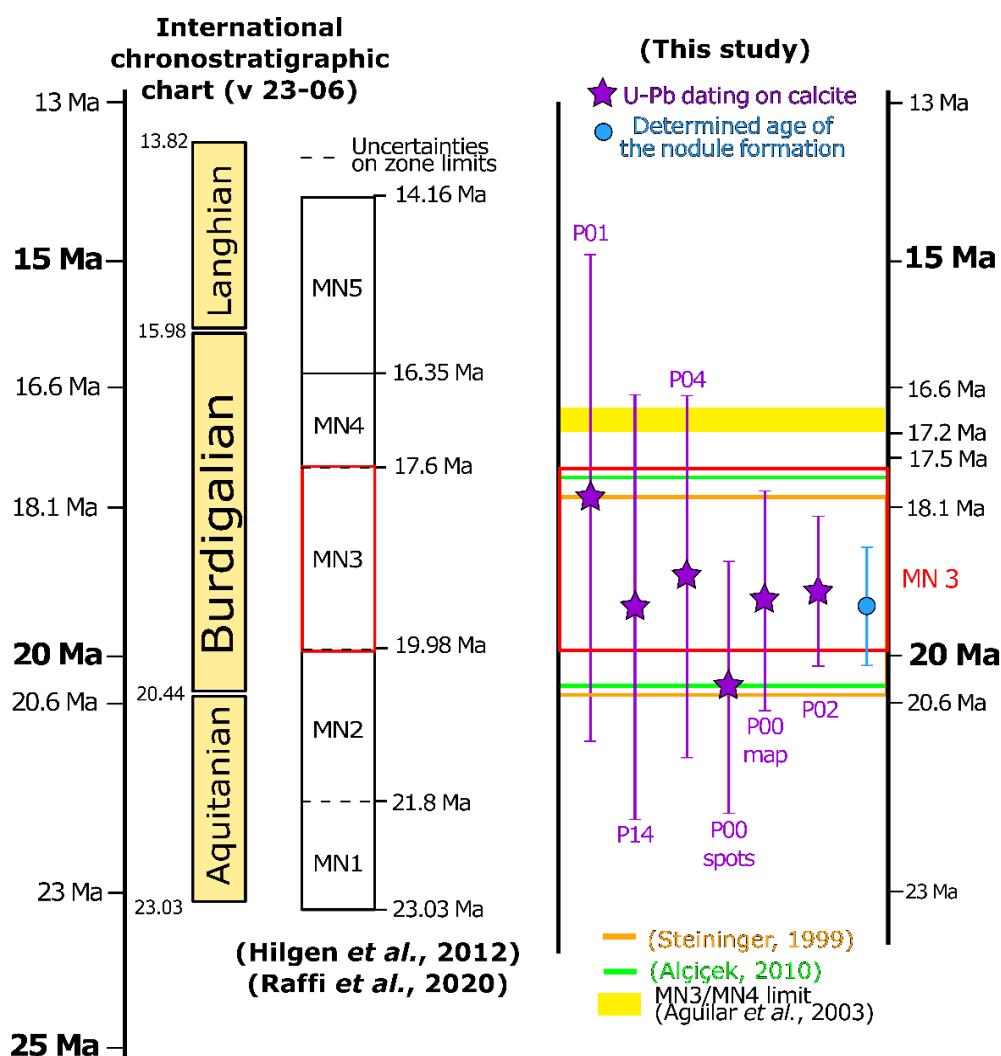


Figure 9: Overview of MN timescales in the literature compared to the age data from this study. The red box defining the MN3 biozone is taken from Raffi et al., (2020).



370 **6 Conclusions**

The application of LA-ICP-MS U-Pb dating of carbonate pedogenic nodules as employed in this study is an efficient and reliable way to provide absolute age data for terrestrial strata. Our samples yield a precise and accurate age of 19.34 ± 0.73 Ma in accordance with earlier biostratigraphic estimates (Orleanian), demonstrating the suitability of the method and confirming the feasibility of the technique to dating continental sedimentary facies that do not contain any index fossils or volcanic horizons such as lavas or ash beds.

Our results are in good agreement with the biostratigraphic age (MN3 of the Neogene Mammalian timescale) of sedimentary horizon s1 from Mauvières (Gagnaison et al., 2023) and represent the first absolute age constraint for the MN3 unit in France. This absolute age dating approach has the potential to advance chronostratigraphy and climatic reconstructions (Liivamägi et al., 2021) by improving inter-basin correlations in continental successions and extending such correlations to the marine sedimentary record.

Author contribution

VM contributed to the conceptualisation, the formal acquisition, the investigation, the methodology, the project administration, the visualisation and the writing (initial draft and edits). RR contributed to the conceptualisation, the formal acquisition, the investigation, the methodology, the project administration, the visualisation and the writing (edits and part of initial draft). KD contributed to the methodology, the supervision and the writing (edits). CG and BM contributed to the resources, the conceptualisation and the writing (edits). RT contributed to the writing (edits). DC contributed to the supervision, the funding acquisition and the writing (edits).

Competing interests

The authors declare that they have no conflict of interest.

390 **Acknowledgments**

The authors would like to acknowledge the Poirier family who allowed us to sample the shell bed (falun) in Mauvières quarry. We would also like to thank Didier Memeteau and Bruno Cossard for assistance sampling the nodules. We acknowledge the support of Science Foundation Ireland, the Environmental Protection Agency, and Geological Survey Ireland under Investigators Programme grant 15/IA/3024.

395



References

- Agnini, C., Fornaciari, E., Raffi, I., Catanzariti, R., Pälke, H., Backman, J., and Rio, D.: Biozonation and biochronology of Paleogene calcareous nannofossils from low and middle latitudes, *Newsletter on Stratigraphy*, 47(2), 131-181. <https://doi.org/10.1127/0078-0421/2014/0042>, 2014.
- 400 Aguilar, J. P., Antoine, P. O., Crochet, J. Y., López Martínez, N., Métais, G., Michaux, J., and Welcomme, J. L.: Les mammifères du Miocène inférieur de Beaulieu (Bouches-du-Rhône, France), comparaison avec Wintershof-West et le problème de la limite MN3/MN4, *Coloquios de paleontología*, Vol. E (1), 1-24, ISSN 1132-1660, 2003.
- Agustí, J., Cabrera, L., Garcés, M., Krijgsman, W., Oms, O., and Parés, J. M.: A Calibrated Mammal Scale for the Neogene of Western Europe, *State of the Art. Earth-Science Reviews*, 52(4), 247-60, [https://doi.org/10.1016/S0012-](https://doi.org/10.1016/S0012-8252(00)00025-8)
405 8252(00)00025-8, 2001.
- Alçiçek, H.: Stratigraphic Correlation of the Neogene Basins in Southwestern Anatolia: Regional Palaeogeographical, Palaeoclimatic and Tectonic Implications, *Palaeogeography, Palaeoclimatology, Palaeoecology* 291(3), 297-318, <https://doi.org/10.1016/j.palaeo.2010.03.002>, 2010.
- Alonso-Zarza, A. M.: Palaeoenvironmental significance of palustrine carbonates and calcretes in the geological record, *Earth-Science Reviews*, 60, 261-298, [https://doi.org/10.1016/S0012-8252\(02\)00106-X](https://doi.org/10.1016/S0012-8252(02)00106-X), 2003.
410
- Bain, R.J., and Foos, A.M.: Carbonate microfabrics related to subaerial exposure and paleosol formation. In *Carbonate Microfabrics: Frontiers in Sedimentology* (Rezak, R.; Lavoie, D.L.; editors), Springer-Verlag: 17-27, 1993.
- Becker, M.L., Rasbury, E.T., Hanson, G.N., and Meyers, W.J.: Refinement in the age of the Carboniferous-Permian boundary based on U-Pb dating of biostratigraphically constrained syn-sedimentary carbonates in the Appalachian region of North America, *Newsletter on Carboniferous Stratigraphy*, 19, 18–20, 2001.
415
- Chew, D., Drost, K., Marsh, J. H. and Petrus, J. A.: LA-ICP-MS imaging in the geosciences and its applications to geochronology, *Chemical Geology*, 559, 119917, <https://doi.org/10.1016/j.chemgeo.2020.119917>, 2021.
- Cohen, K.M., Finney, S.C., Gibbard, P.L. and Fan, J.-X.: The ICS International Chronostratigraphic Chart, *Episodes* 36, 199-204, 2013; updated(09/23).



- 420 Daxner-Höck, G., Badamgarav, D., Barsbold, R., Bayarmaa, B., Erbajeva, M., Göhlich, U. B., Harzhauser, M., Höck, E., Höck, V., Ichinnorov, N., Khand, Y., López-Guerrero, P., Maridet, O., Neubauer, T., Oliver, A., Piller, W., Tsogtbaatar, K. and Ziegler, R.: Oligocene stratigraphy across the Eocene and Miocene boundaries in the Valley of Lakes (Mongolia), *Palaeobiodiversity and Palaeoenvironments*, 97, 111-218, 2017.
- Drake, H., Mathurin, F. A., Zack, T., Schäfer, T., Roberts, N. M. W., Whitehouse, M., Karlsson, A., Broman, C., and
425 Åström, M. E.: Incorporation of Metals into Calcite in a Deep Anoxic Granite Aquifer, *Environmental Science & Technology*, 52, 493-502, [10.1021/acs.est.7b05258](https://doi.org/10.1021/acs.est.7b05258), 2018.
- Drost, K., Chew, D., Petrus, J. A., Scholze, F., Woodhead, J. D., Schneider, J. W. and Harper, D. A. T.: An image mapping approach to U-Pb LA-ICP-MS carbonate dating and applications to direct dating of carbonate sedimentation, *Geochemistry, Geophysics, Geosystems*, 19, 4631-4648, <https://doi.org/10.1029/2018gc007850>, 2018.
- 430 Engesser, B. and Mödden, C.: A new version of the biozonation of the Lower Freshwater Molasse (Oligocene and Agenian) of Switzerland and Savoy on the basis of fossil mammals. In: Aguilar, J.-P., Legendre, S. and Michaux, J., eds. *Biochrom'97 Montpellier*, Ecole pratique des hautes études, Institut de Montpellier, Montpellier (France), 475-499, 1997.
- Esteban, M., and Klappa, C. F.: Subaerial exposure environment: Chapter 1: Part 2. In: Scholle, P. A., Bebout, D.G. and
435 Moore C.H., eds. *Carbonate Depositional Environments*, 23-54, <https://doi.org/10.1306/M33429C1>, 1983.
- Ezquerro, L., Luzón, A., Simón, J.L., and Liesa, C.L.: A review of the European Neogene Mammal zones from integration of litho-, bio- and magnetostratigraphy in the Teruel Basin, *Earth-Science Reviews*, 234, 104223, <https://doi.org/10.1016/j.earscirev.2022.104223>, 2022.
- Fortelius, M., Eronen, J.T., Kaya, F., Tang, H., Raia, P., and Puolamäki, K.: Evolution of Neogene Mammals in Eurasia:
440 Environmental forcing and biotic interactions, *Annual Review of Earth and Planetary Sciences*, 42, 579-604, <https://doi.org/10.1146/annurev-earth-050212-124030>, 2014.
- Fournier, F., Montaggioni, L., and Borgomano, J.: Palaeoenvironments and high-frequency cyclicity from Cenozoic South-East Asian shallow-water carbonates: a case study from the Oligo-Miocene buildups of Malampaya (Offshore Palawan, Philippines), *Marine and Petroleum Geology*, 21, 1-21, <https://doi.org/10.1016/j.marpetgeo.2003.11.012>, 2004.



- 445 Gagnaison, C.: Le Miocène du Nord-Ouest de la France (vallée de la Loire, Bretagne et Normandie) : Révision du contexte taphonomique des fossiles de vertébrés, proposition d'un découpage stratigraphique et clarification des variations paléoenvironnementales, *Fossiles*, 41, 3-30, 2020.
- Gagnaison, C., Cabidoche, M., Riera, R., Dechamps, M., and Gagnaison, J.C.: The geological context of the Lower Orleanian continental sands from the Savigné-sur-Lathan/Noyant-sous-le-Lude basin (Anjou-Touraine, France),
- 450 *Bulletin d'Information des Géologue du Bassin de Paris*, 57, 3-15, 2020.
- Gagnaison, C., Mennecart, B., Bailleul, J., Barrier, P., Chenot, E., Toullec, R., Potel, S., Martin, H., Millet, A. and Memeteau, D. : Nouvelles données géologiques et biostratigraphiques du gisement paléontologique à vertébrés de Mauvières, à Marcilly-sur-Maulne (Miocène inférieur et moyen ; Indre-et-Loire, France), *Geodiversitas*, 45(16), 449-478, <https://doi.org/10.5252/geodiversitas2023v45a16>, 2023.
- 455 Galbraith, R. F., Roberts, R.G., Laslett, R.G., Yoshida, H., and Olley, J.M.: Optical dating of single and multiple grains of quartz from Jinmium rock shelter, northern Australia: part 1, experimental design and statistical models, *Archaeometry*, 41(2), 339-364, <https://doi.org/10.1111/j.1475-4754.1999.tb00987.x>, 1999.
- Gates-Rector, S., and Blanton, T.: The Powder Diffraction File: A quality materials characterization database, *Powder Diffraction*, 34(4), 352-360, <https://doi.org/10.1017/S0885715619000812>, 2019.
- 460 Getty, S. R., Asmerom, Y., Quinn, T. M., and Budd, A. F.: Accelerated Pleistocene coral extinctions in the Caribbean Basin shown by uranium-lead (U-Pb) dating, *Geology*, 29(7), 639–642, <https://doi.org/10.1130/0091-7613>, 2001.
- Ginsburg, L.: Les faunes de mammifères terrestres du Miocène moyen des Faluns du bassin de Savigné-sur-Lathan (France), *Geodiversitas*, 23, 381-394, 2001.
- Ginsburg L., Cheneval J., Janvier P., Pouit D. and Sen S.: Les vertébrés des sables continentaux d'âge orléanien inférieur
- 465 (MN3) de Mauvières à Marcilly-sur-Maulne (Indre-et-Loire), La Brosse à Meigné-le-Vicomte (Maine-et-Loire) et Chitenay (Loir-et-Cher), *Geodiversitas*, 22(4), 597-631, 2000.
- Guillocheau, F., Robin, C., Allemand, P., Bourquin, S., Brault, N., Dromart, G., Friedenber, R., Garcia, J.-P., Gaulier, J.-M., Gaumet, F., Grosdoy, B., Hanot, F., Le Strat, P., Mettraux, M., Nalpas, T., Prijac, C., Rigollet, C., Serrano, O., and



- Grandjean, G.: Meso-Cenozoic geodynamic evolution of the Paris Basin: 3D stratigraphic constraints, *Geodinamica Acta*, 13, 189-246, [https://doi.org/10.1016/S0985-3111\(00\)00118-2](https://doi.org/10.1016/S0985-3111(00)00118-2), 2000.
- Hilgen, F. J., Lourens, L. J., Van Dam, J. A., Beu, A. G., Boyes, A. F., Cooper, R. A., Krijgsman, W., Ogg, J. G., Piller, W. E. and Wilson, D. S.: Chapter 29 - The Neogene Period. In: Gradstein, F. M., Ogg, J. G., Schmitz, M. D. and Ogg, G. M. (eds.), *The Geologic Time Scale*, Boston, Elsevier, 2012.
- Hoff, J.A., Jameson, J., and Hanson, G.N.: Application of Pb isotopes to the absolute timing of regional exposure events in carbonate rocks; an example from U-rich dolostones from the Wahoo Formation (Pennsylvanian), Prudhoe Bay, Alaska, *Journal of Sedimentary Research*, 65, 225–233, <https://doi.org/10.1306/D426807C-2B26-11D7-8648000102C1865D>, 1995.
- Hugueney, M.: Genera *Euricetodon* and *Pseudocricetodon*. In Rössner, G.,E., and Heissig K., (eds.), *The Miocene Land Mammals of Europe*. Verlag Dr. Friedrich Pfeil, München: 347-358, 1999.
- Kerr, R. A.: Huge impact tied to mass extinction, *Science*, 257, 878-880, 1992.
- Li, Q., Parrish, R. R., Horstwood, M. S. A., and McArthur, J. M.: U–Pb dating of cements in Mesozoic ammonites: *Chemical Geology*, 376, 76-83, <http://dx.doi.org/10.1016/j.chemgeo.2014.03.020>, 2014.
- Liivamägi, S., Środoń, J., Bojanowski, M.J., Stanek, J.J., and Roberts, N.M.W.: Precambrian paleosols on the Great Unconformity of the East European Craton: An 800 million year record of Baltica’s climatic conditions, *Precambrian Research*, 363, 106327, <https://doi.org/10.1016/j.precamres.2021.106327>, 2021.
- Luczaj, J.A., and Goldstein, R.H.: Diagenesis of the Lower Permian Krider Member, Southwest Kansas, U.S.A.: Fluid-Inclusion, U-Pb, and Fission-Track Evidence for Reflux Dolomitization During Latest Permian Time, *Journal of Sedimentary Research*, 70, 762–773, <https://doi.org/10.1306/2DC40936-0E47-11D7-8643000102C1865D>, 2000.
- Ludwig, K. R.: User’s manual for Isoplot 3.75, Berkley Geochronology Center Special Publication, 5, 1–75, 2012.
- Mein, P.: Report on activity RCMNS-Working groups (1971–1975), pp. 78–81, Bratislava, 1975.
- Mein P.: European Miocene Mammal Biochronology. In Rössner, G.,E., and Heissig K., (eds.), *The Miocene Land Mammals of Europe*. Verlag Dr. Friedrich Pfeil, München, 25-38, 1999.



- Methner, K., Mulch, A., Fiebig, J., Wacker, U., Gerdes, A., Graham, S.A., and Chamberlain, C.P.: Rapid Middle Eocene temperature change in western North America, *Earth and Planetary Science Letters*, 450, 132–139, 495 <https://doi.org/10.1016/j.epsl.2016.05.053>, 2016.
- Monchal, V., Drost, K., and Chew, D.: Precise U-Pb dating of incremental calcite slickenfiber growth: Evidence for far-field Eocene fold reactivation in Ireland, *Geology*, 51, 611-615, <https://doi.org/10.1130/G50906.1>, 2023.
- Monchal, V., Rateau, R., Drost, K., Gagnaison, C., Mennecart, B., Toullec, R., & Chew, D.: Supplementary Tables : U-Pb direct dating on calcite paleosol nodules: first absolute age constraints on the Miocene continental succession of the Paris Basin [Data set], Zenodo, <https://doi.org/10.5281/zenodo.12799549>, 2024. 500
- Montano, D., Gasparini, M., Gerdes, A., Della Porta, G. and Albert, R.: In-situ U-Pb dating of Ries Crater lacustrine carbonates (Miocene, South-West Germany): Implications for continental carbonate chronostratigraphy, *Earth and Planetary Science Letters*, 568, 117011, 2021.
- Nuriel, P., Weinberger, R., Kylander-Clark, A.R.C., Hacker, B.R., and Craddock, J. P.: The onset of the Dead Sea transform based on calcite age-strain analyses, *Geology*, 45(7), 587-590, <https://doi.org/10.1130/G38903.1>, 2017. 505
- Parrish, R. R., Parrish, C. M., and Lasalle, S.: Vein calcite dating reveals Pyrenean orogen as cause of Paleogene deformation in southern England, *Journal of the Geological Society*, 175(3), 425–442, <https://doi.org/10.1144/jgs2017-107>, 2018.
- Perry, C. T. and Taylor, K. G.: Inhibition of dissolution within shallow water carbonate sediments: impacts of terrigenous sediment input on syn-depositional carbonate diagenesis, *Sedimentology*, 53, 495-513, <https://doi.org/10.1111/j.1365-3091.2006.00777.x>, 2006. 510
- Poujol, M., Mercuzot, M., Lopez, M., Bourquin, S., Bruguier, O., Hallot, E. & Beccaletto, L.: Insights on the Permian tuff beds from the Saint-Affrique Basin (Massif Central, France): an integrated geochemical and geochronological study, *Comptes Rendus. Géoscience*, 355, 137-161, 2023.
- Raffi, I., Wade, B. S., Pälke, H., Beu, A. G., Cooper, R., Crundwell, M. P., Krijgsman, W., Moore, T., Raine, I., Sardella, R. and Vernyhorova, Y. V.: Chapter 29 - The Neogene Period. In: Gradstein, F. M., Ogg, J. G., Schmitz, M. D. and Ogg, G. M. (eds.), *Geologic Time Scale 2020*, Elsevier, 2020. 515



- Rasbury, E.T., and Cole, J.M.: Directly dating geologic events: U-Pb dating of carbonates, *Reviews of Geophysics*, 47, RG3001, <https://doi.org/10.1029/2007RG000246>, 2009.
- 520 Rasbury, E.T., Hanson, G.N., Meyers, W.J., Holt, W.E., Goldstein, R.H., and Saller, A.H.: U-Pb dates of paleosols: Constraints on late Paleozoic cycle durations and boundary ages, *Geology*, 26, 403–406, <https://doi.org/10.1130/0091-7613>, 1998.
- Rasbury, E.T., Hanson, G.N., Meyers, W.J., and Saller, A.H.: Dating of the time of sedimentation using U-Pb ages for paleosol calcite, *Geochimica et Cosmochimica Acta*, 61, 1525–1529, [https://doi.org/10.1016/S0016-7037\(97\)00043-4](https://doi.org/10.1016/S0016-7037(97)00043-4),
525 1997.
- Rasbury, E.T., Meyers, W.J., Hanson, G.N., Goldstein, R.H., and Saller, A.H.: Relationship of Uranium to Petrography of Caliche Paleosols with Application to Precisely Dating the Time of Sedimentation, *Journal of Sedimentary Research*, 70, 604–618, <https://doi.org/10.1306/2DC4092B-0E47-11D7-8643000102C1865D>, 2000.
- Rasbury, E. T., Piccione, G., Holt, W., and Ward, W. B.: Potential for constraining sequence stratigraphy and cycle
530 stratigraphy with U-Pb dating of carbonates, *Earth-Science Reviews*, 243, 104495, <https://doi.org/10.1016/j.earscirev.2023.104495>, 2023.
- Roberts, N. M. W. and Walker, R. J.: U-Pb geochronology of calcite-mineralized faults: Absolute timing of rift-related fault events on the northeast Atlantic margin, *Geology*, 44(7), 531-534, <https://doi.org/10.1130/G37868.1>, 2016.
- Roberts, N. M. W., Drost, K., Horstwood, M. S. A., Condon, D. J., Chew, D., Drake, H., Milodowski, A. E., McLean, N. M.,
535 Smye, A. J., Walker, R. J., Haslam, R., Hodson, K., Imber, J., Beaudoin, N., and Lee, J. K.: Laser ablation inductively coupled plasma mass spectrometry (LA-ICP-MS) U–Pb carbonate geochronology: strategies, progress, and limitations, *Geochronology*, 2, 33–61, <https://doi.org/10.5194/gchron-2-33-2020>, 2020.
- Roberts, N. M. W., Žák, J., Vacek, F. and Sláma, J.: No more blind dates with calcite: Fluid-flow vs fault-slip along the Očkov thrust, Prague Basin, *Geoscience Frontiers*, 12, 101143, <https://doi.org/10.1016/j.gsf.2021.101143>, 2021.
- 540 Roberts, N. M. W. and Holdsworth, R. E.: Timescales of faulting through calcite geochronology: A review, *Journal of Structural Geology*, 158, 104578, <https://doi.org/10.1016/j.jsg.2022.104578>, 2022.



- Smith, P. E. and Farquhar, R. M.: Direct dating of Phanerozoic sediments by the ^{238}U – ^{206}Pb method, *Nature*, 341, p. 518, 1989.
- Steininger F, F.: Chronostratigraphy, geochronology and biochronology of the Miocene "European Land Mammal Mega-Zones" (ELMMZ) and the Miocene "Mammal-Zones (MN-Zones)". In: Rössner, G. E. and Heissig, K. (eds.) *The Miocene : Land Mammals of Europe*, 9-24, Friedrich Pfeil, 1999.
- Subarkah, D., Nixon, A. L., Gilbert, S. E., Collins, A. S., Blades, M. L., Simpson, A., Lloyd, J. C., Virgo, G. M., and Farkaš, J.: Double dating sedimentary sequences using new applications of in-situ laser ablation analysis, *Lithos*, 480-481, 107649, <https://doi.org/10.1016/j.lithos.2024.107649>, 2024.
- 550 Temey, I.: *Le Néogène de Touraine: approche environnementale et paléogéographique des faluns du bassin de Noyant-Savigné (Indre-et-Loire et Maine-et-Loire, France)*, Mémoire d'Ingénieur géologue, Institut Géologique Albert-de-Lapparent, Cergy-Pontoise, 73, 292p, 1996.
- Van Dam, J. A., Alcalá, L., Zarza, A. A., Calvo, J. P., Garcés, M., and Krijgsman, W.: The Upper Miocene Mammal Record from the Teruel-Alfambra Region (Spain). The MN System and Continental Stage/Age Concepts Discussed, *Journal of Vertebrate Paleontology*, 21(2), 367–385, <http://www.jstor.org/stable/20061959>, 2001.
- 555 Van der Meulen, A.J., García-Paredes, I., Álvarez-Sierra, M.A., Van den Hoek Ostende, L.W., Hordijk, K., Oliver, A., and Peláez-Campomanes, P.: Updated Aragonian biostratigraphy: Small Mammal distribution and its implications for the Miocene European Chronology, *Geologica Acta*, 10(2), 159-179, <https://doi.org/10.1344/105.000001710>, 2012.
- Vermeesch, P.: IsoplotR: A free and open toolbox for geochronology, *Geoscience Frontiers*, 9, 1479-1493, <https://doi.org/10.1016/j.gsf.2018.04.001>, 2018.
- 560 Wang, Z.S., Rasbury, E.T., Hanson, G.N., and Meyers, W.J.: Using the U-Pb system of calcretes to date the time of sedimentation of clastic sedimentary rocks, *Geochimica et Cosmochimica Acta*, 62, 2823–2835, [https://doi.org/10.1016/S0016-7037\(98\)00201-4](https://doi.org/10.1016/S0016-7037(98)00201-4), 1998.
- Winter, B.L., and Johnson, C.M.: U-Pb dating of a carbonate subaerial exposure event, *Earth and Planetary Science Letters*, 131, 177–187, [https://doi.org/10.1016/0012-821X\(95\)00026-9](https://doi.org/10.1016/0012-821X(95)00026-9), 1995.
- 565



Wright, V. P.: Paleosols. Their Recognition and Interpretation, Princeton University Press, Blackwell Scientific, Oxford, 1987.

Wright, V. P.: A micromorphological classification of fossil and recent calcic and petrocalcic microstructures. In: Douglas, L. A. (eds.) Soil Micromorphology. Proceedings of 8th meeting of Soil Micromorphology, San Antonio, 1988 .

570 Developments in Soil Science, 19, Elsevier, Amsterdam, 401–407, 1990.

Zamanian, K., Pustovoytov, K., Kuzyakov, Y.: Pedogenic carbonates: Forms and formation processes, Earth-Science Reviews, 157, 1-17, <http://dx.doi.org/10.1016/j.earscirev.2016.03.003>, 2016.